

- Chem. **92**, 4009 (1988).
- ³⁷J. C. Pinegar, J. D. Langenberg, C. A. Arrington, E. M. Spain, and M. D. Morse, *J. Chem. Phys.* **102**, 666 (1995).
- ³⁸E. A. Rohlfing and J. J. Valentini, *J. Chem. Phys.* **84**, 6560 (1986).
- ³⁹K. P. Huber and G. Herzberg, *Constants of Diatomic Molecules* (Van Nostrand Reinhold, New York, 1979), Vol. 4.
- ⁴⁰A. M. James, P. Kowalczyk, R. Fournier, and B. Simard, *J. Chem. Phys.* **99**, 8504 (1993).
- ⁴¹D. A. Hales, L. Lian, and P. B. Armentrout, *Int. J. Mass Spectrom. Ion Processes* **102**, 269 (1990).
- ⁴²S. Lee, D. M. Bylander, and L. Kleinman, *Phys. Rev. B* **37**, 10035 (1988).
- ⁴³M. D. Morse, *Chem. Rev. (Washington, D.C.)* **86**, 1049 (1986).
- ⁴⁴J. D. Langenberg and M. D. Morse, *J. Chem. Phys.* **108**, 2331 (1998).

All-electron calculations on MgO cluster (n=1-10) with Tohoku University Mixed-Basis Program TOMBO

Amit Jain*, Vijay Kumar** and Yoshiyuki Kawazoe*

* Institute for Materials Research, Tohoku University, 2-1-1 Katahira, Aoba-ku, Sendai 980-8577, Japan

Fax: 81-22-215-2052, e-mail: amitjain@imr.edu

** Dr. Vijay Kumar Foundation, 45 Bazaar Street, K. K. Nagar (West), Chennai 600 078, India

All-electron mixed-basis approach which uses both plane wave and atomic orbitals as the basis functions, has been used to do *ab initio* study of $(\text{MgO})_n$ cluster $n=1-10$. For this purpose Tohoku Mixed-Basis Program TOMBO based on the local density approximation (LDA) is used to optimize the structures of MgO clusters. Calculated electronic structures and bond length are in good agreement with available experiment data. TOMBO program, when used in parallel environment, makes the structure optimization calculation quite fast with increase in MgO cluster size.

Key words: MgO Clusters, all-electron mixed-basis method, structure optimization, parallel processing

1. INTRODUCTION

Currently there is much focus on materials research at the nanoscale because of the important role these are expected to play in future technologies. It is important to develop a fundamental understanding of the growth behavior of matter in going from atoms to bulk. As the structures and bonding at the nanoscale are generally different from bulk, studies of clusters provide an interesting way to understand the evolution of the properties of materials from atoms to the bulk condensed state. Therefore, this has prompted numerous studies of cluster properties as a function of size.

Recently there has been an intense interest in the study of metal oxide clusters. Often clusters of such compounds are considered to be bulk fragments. However, their structure and properties could be different at the nanoscale. Here we consider clusters of magnesium oxide. There have been very few *ab initio* studies on small MgO clusters^{[1][4]}. Also empirical methods have been used considering primarily ionic bonding^[5]. However, the understanding of the growth behavior is still not well understood. A survey of the previous studies gave a very contradictory view of the MgO cluster structures and bonding behavior. In this light we studied MgO clusters using all electron mixed basis approach. As one expects significant charge transfer from Mg atoms to O, it is considered appropriate to include the inner orbitals that are best represented in an all electron calculation. For this, we have used Tohoku University Mixed-Basis program TOMBO for optimizing the MgO cluster structures.

2. ALL-ELECTRON MIXED-BASIS METHOD TOMBO

The mixed-basis means that the combination of both plane waves (PWs) and atomic orbitals (AOs) is used as basis function. The introduction of AOs considerably reduces the load of the PW expansion method^{[7][8]}. In the mixed-basis method, the electronic wavefunctions are expanded using both PWs and AOs, making an accurate description of both local and extended

electronic states, where not only valence AOs but also core AOs are incorporated to describe all-electrons without using pseudopotentials.

In present study, structure optimization of MgO clusters has been done using TOMBO, which is a program based on all-electron mixed basis method developed at Tohoku University. TOMBO uses optimal linear and Broyden mixing of the electronic charge density and can be used to do structural optimization and molecular dynamic simulations, vibrational analysis, including IR activity, Born effective charges and can simulate Fermi contact interaction and dipole moment. In TOMBO the Coulomb and exchange-correlation potentials are evaluated separately for PW and for AO, respectively, in reciprocal space and in real space. So PW-PW, AO-PW and AO-AO contributions to the charge density and the potential are calculated separately^[9]. We have used local density approximation (LDA) for this study.

To take advantage of the multiprocessor architectures of most modern supercomputers, TOMBO code has been SIMD-parallelized by means of message passing interface (MPI) calls in the most computationally demanding subroutines e.g. for computing the product of the Hamiltonian and the wavefunction, for computing FFTs, for orthogonalizing the Hamiltonian, and for transforming the representation of the wavefunction on orthogonal and non-orthogonal bases^[9]. TOMBO program is capable of very large scale calculations when used in parallel computing environment^[10].

3. RESULTS AND DISCUSSION

3.1 Structures

We calculated the optimized clusters of MgO with LDA. The unit cell is chosen as a cube of 1.6 nm width. We have used Hitachi SR8000/64 512 parallel 1 teraflop supercomputer to do these all-electron mixed basis calculations.

The results of the structures of different isomers studied here, as well as bond length, total energy and energy per molecule are given in Fig. 1, Fig. 2, Table I

and Table II. The red balls represent Oxygen and green balls represent Magnesium in Fig. 1 and Fig. 2.

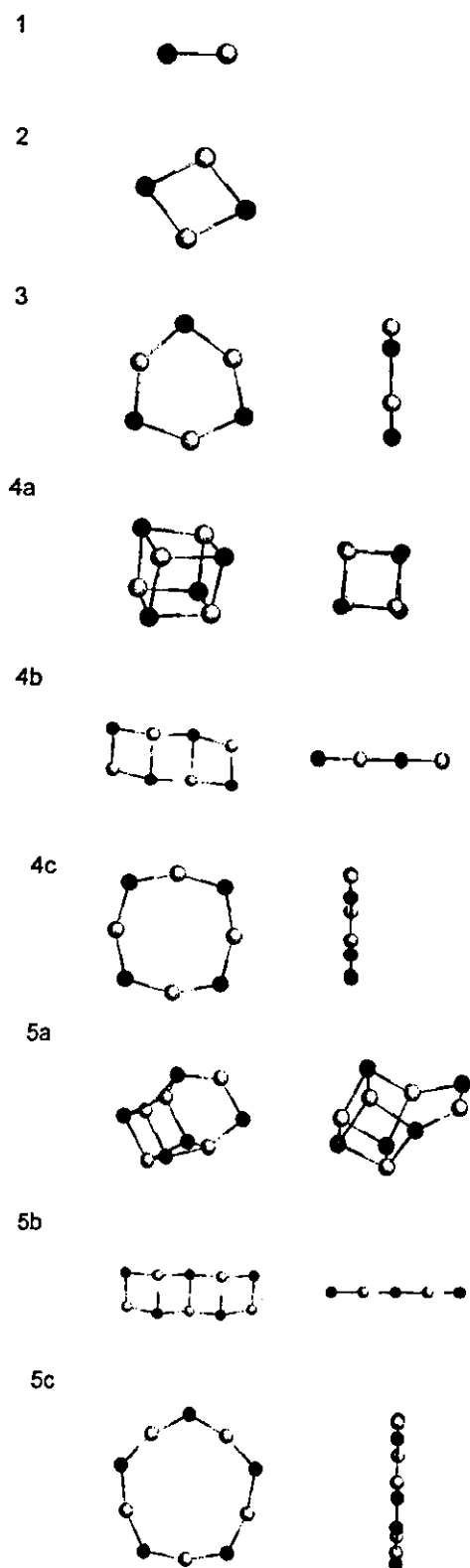


Fig. 1 Optimized structures of MgO $n=1-5$. From $n=3-5$ front view is shown in the left side and side view of the structures is shown in right side

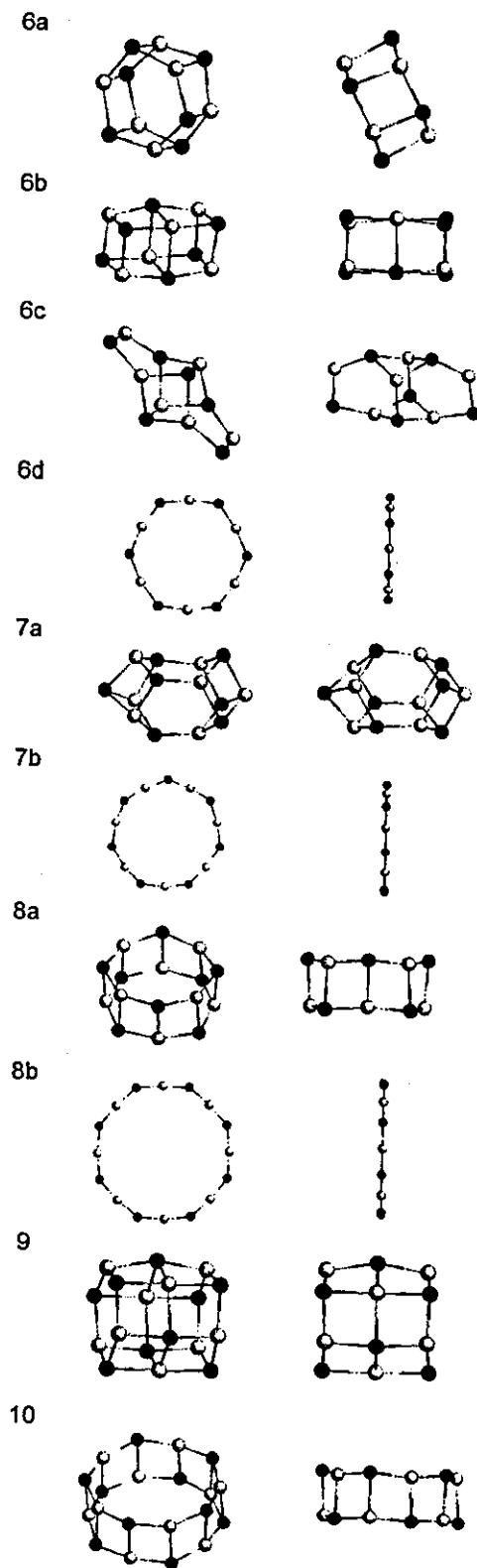


Fig. 2 Optimized structures of MgO $n=6-10$. Front/top view is shown in the left side and side view of the structures is shown in right side

Table I Structure and Bond length (Å) of MgO clusters

n	structure	Bond length (Å)
1	monomer	1.75
2	2*2*1	1.88
3	ring	1.83
4a	2*2*2	1.95
4b	4*2*1	1.84, 2.08, 1.91, 1.85, 1.89
4c	ring	1.82
5a	distorted cube open at one side	1.94, 1.93, 1.95, 1.97, 1.98, 1.86, 1.80, 1.89
5b	5*2*1	1.84, 2.09, 1.99, 1.85, 1.91, 1.89
5c	ring	1.815
6a	ring*2	1.91, 1.99
6b	3*2*2	1.94, 2.11, 1.91, 1.97
6c	distorted cube open at two sides	1.81, 1.90, 1.86, 1.89, 1.96, 1.98
6d	ring	1.81
7a	cage	1.93, 1.94, 1.87
7b	ring	1.80
8a	ring*2	1.89, 2.00
8b	ring	1.80
9	ring*3	1.90, 2.05
10	ring*2	1.89, 2.00

Table II Total energy (eV) and Energy per MgO molecule (eV) for MgO clusters n=1-10

n	Total Energy	Energy/molecule
1	7440.07	7440.07
2	14896.74	7448.37
3	22348.29	7449.43
4a	29800.68	7450.17
4b	29799.41	7449.85
4c	29799.00	7449.75
5a	37251.22	7450.24
5b	37250.80	7450.16
5c	37249.33	7449.87
6a	44704.70	7450.78
6b	44704.58	7450.76
6c	44701.85	7450.31
6d	44699.53	7449.92
7a	52156.30	7450.90
7b	52149.66	7449.95
8a	59607.71	7450.96
8b	59600.12	7450.02
9	67061.00	7451.22
10	74510.29	7451.03

When these results are compared with the experimental results, calculated bond length of the MgO monomer is in excellent agreement with the corresponding experimental data^{[1],[11]}.

It is clear from the optimized structures shown in Fig.1 and Fig 2 and calculated total energy of these optimized structures that MgO clusters prefer 3-dimensional structures from (MgO)₄ onward. A very important observation from the optimized 3-d structures is the chair type structure of MgO clusters from n ≥ 4. The chair kind structures more clearly visualized in the

side views of the structures and more clearly observed in the side views of the fig. 4a, 6a, 6b, 8a, 9, 10. This is very interesting as this indicates the existence of some covalent bonding in MgO cluster where as MgO is considered ionic in bulk state. It is also interesting to note that the optimized planer isomers of MgO clusters have larger angle on Magnesium than Oxygen though the bond length remains same within each plan structure.

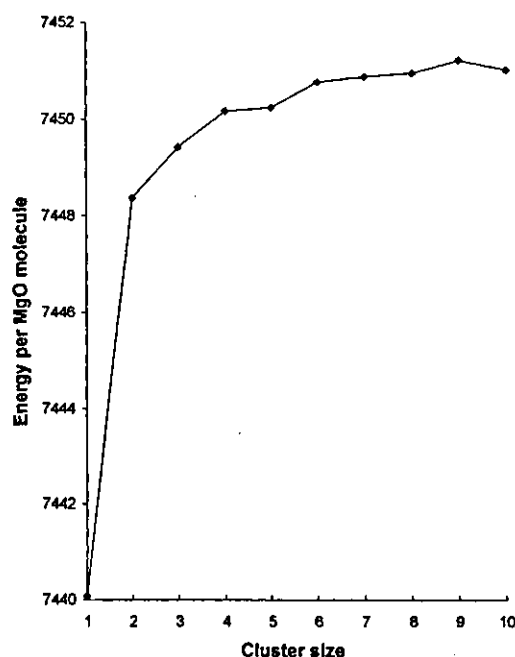


Fig.3 Energy per MgO molecule for the most stable MgO clusters.

The energy per MgO molecule graph with the variation of cluster size, shown in Fig. 3 indicates that Cluster 2, 4, 6 and 9 are more preferable than the other clusters. These results are in full agreement with the mass spectra of MgO clusters^[5], which gives the MgO magic clusters at n=2, 4, 6 and 9.

3.2 Parallelized Calculation for MgO Cluster Study

Some *ab initio* simulations for MgO cluster structure optimization have been done on different number of Hitachi SR8000 super computer nodes. Time taken in these simulations has shown the effectiveness of the TOMBO parallelization. A typical comparison of total time taken in structure optimization for (MgO)₃ and (MgO)₉ clusters when same structure of (MgO)₃ and (MgO)₉ is optimized with different number of computer nodes in parallel is shown below in Fig. 4

In case of (MgO)₃ time saving is not much because time utilized in communicating between different nodes is significant when compared to the actual time saving due to the parallel computation in different nodes. But in case of (MgO)₉ there is a significant time saving when number of nodes are increased. The reason for this is that the communication time between different nodes is not comparable to the actual time saving in the computation process due to the use of parallel nodes. As the size of cluster increases, we need more

computational resources and time and we will be able to save more time if using the parallel computing nodes for these larger calculations.

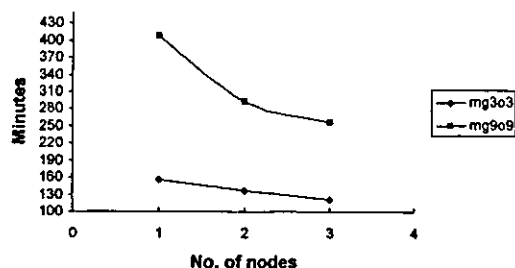


Fig. 4 Time taken for structure optimization of $(\text{MgO})_3$ and $(\text{MgO})_9$ using different number of parallel computer nodes.

4. CONCLUSIONS

In summary, we have reported results of our all-electron mixed-basis calculations using TOMBO. We have reported various isomers and the lowest energy structures of MgO clusters ($n=1-10$), which are in excellent agreement with the experimental results available. Another important conclusion of our study from the finally optimized structure is the indication of covalent bonding in MgO clusters whereas MgO is considered ionic in bulk state. We have found magic clusters of MgO at $n=2, 4, 6, 9$ which are also fully in agreement with the mass spectra. Our calculations also show that the structure optimization through TOMBO is quite fast when used in parallel mode with many parallel computer nodes, which is very important for the further study of large size clusters.

5. ACKNOWLEDGEMENTS

The authors would like to thank the staff of the Center for Computational Materials Science at the Institute for Materials Research, Tohoku University for

making the Hitachi SR8000/64 parallel machines available and for their cooperation. We are also grateful for helpful discussions with Dr. Marcel Sluiter and Dr. Umesh V. Waghmare. A. J. is grateful for the support of the Japan Society for the Promotion of Science. V. K. thankfully acknowledges the kind hospitality at the Institute for Materials Research.

6. REFERENCES

- [1] J. M. Recio and R. Pandey, *Phys. Rev. A*, **47**, 2075-82 (1993).
- [2] M.-J. Malliavin and C. Coudray, *J. Chem. Phys.*, **106**, 2323-30 (1997).
- [3] E. d. I. Puente, A. Aguado, A. Ayuela and J. M. Lopez, *Phys. Rev. B*, **56**, 7607-14, (1997).
- [4] M. Gutowski, P. Skurski, X. Li and L.-S. Wang, *Phys. Rev. Lett.*, **85**, 3145-48, (2000).
- [5] P. J. Ziemann and A. W. Castleman, Jr., *J. Chem. Phys.*, **94**, 718-28 (1991).
- [6] T. Bredow, G. Geudtner and K. Jug, *J. Chem. Phys.*, **105**, 6395-400 (1996).
- [7] S. G. Louie, K.-M. Ho and M. L. Cohen, *Phys. Rev. B*, **19**, 1774-82 (1979).
- [8] P. Bendt and A. Zunger, *Phys. Rev. B*, **26**, 3114-37 (1982).
- [9] Marcel Sluiter, "TOMBO Tohoku University Mixed-Basis Program version 1.2c for Clusters", <http://www-lab.imr.edu/~marcel/tombo/tombo.html>, (2003).
- [10] Marcel H. F. Sluiter, Rodion V. Belosludov, Vladimir R. Belosludov, Amit Jain, Hitoshi Adachi, Yoshiyuki Kawazoe, Kenji Higuchi, and Takayuki Otani, "Ab initio Study of Hydrogen Hydrate Clathrates for Hydrogen Storage within the ITBL Environment," Lecture Notes in Computer Science, Springer-Verlag Heidelberg, Germany, (2003), Vol 2858, pp. 330-341.
- [11] K. P. Huber and G. Herzberg, "Molecular Spectra and Molecular Structure, IV. Constants of Diatomic Molecules", Van Nostrand Reinhold, New York, (1979).

(Revised Jan. 7, 2004; Accepted March 31, 2004)

Dielectric Function of (CdSe)₁₃ Clusters

Yoshifumi Noguchi¹, Kaoru Ohno^{1,2}, Vijay Kumar^{3,4}, Yoshiyuki Kawazoe³, Yurii Barnakov², and Atsuo Kasuya²

¹Department of Physics, Graduate School of Engineering, Yokohama National University, 79-5 Tokiwadai, Hodogaya-ku, Yokohama 240-8501, Japan

Fax: 81-45-338-3020, e-mail: d02gd224@ynu.ac.jp, ohno@ynu.ac.jp

²Center for Interdisciplinary Research, Tohoku University, Aramaki, Aoba-ku, Sendai 980-8578, Japan

Fax: 81-22-217-5756, e-mail: kasuya@cir.tohoku.ac.jp

³Institute for Materials Research, Tohoku University, 2-1-1 Katahira, Aoba-ku, Sendai 980-8577

Fax: 81-22-215-2052, e-mail: kumar@imr.edu, kawazoe@imr.edu

⁴Dr. Kumar Foundation, 45 Bazaar Street, K.K. Nagar (West), Chennai 600 078, India.

We investigate theoretically the atomic and electronic structures of (CdSe)₁₃ cluster which is of the smallest magic number size among (CdSe)_n found experimentally recently. Using the first-principles approach based on the local density approximation in the density functional theory, we calculate the dielectric function for two cluster geometries of (CdSe)₁₃ and compare the results with the changes in the optical absorption spectra under the illumination.

Key words: optical absorption spectra, dielectric response function, density functional theory, first principles

1. INTRODUCTION

Quite recently, (CdSe)_n clusters have been synthesized and characterized by the optical and time-of-flight (TOF) mass measurements by Barnakov *et al.*[1,2]. The TOF mass spectra of positive ions show that (CdSe)₁₃ is an abundant magic number cluster. Kumar *et al.* [3] have determined the most stable geometry of the clusters by means of the standard *ab initio* pseudopotential approach based on the local density approximation (LDA) in density functional theory. The magic (CdSe)₁₃ cluster has an endohedral cage structure composed of twelve Se ions at the surface of an icosahedral cage, one Se ion at the center and thirteen Cd ions at slightly inner than the cage surface. The main interest of these clusters lies in their specific behavior in the optical response.

In the present paper, we calculate, for the first time, the dielectric function of (CdSe)₁₃ and compare the results with the optical absorption spectra measured by Kasuya *et al.* [1]. In addition to the most stable cage structure, we consider another structure of (CdSe)₁₃ which can be obtained by cutting the bulk wurtzite and by optimizing their geometrical structures. Throughout this paper, we use *ab initio* methods within the LDA in density functional theory.

2. EXPERIMENT

(CdSe)_n clusters was created by following sequence :

i . Solution of CdNTA and Na₂SeSO₃ was mingled with decylamine (CH₃(CH₂)₉NH₂) as surfactant.

(Cd²⁺ and Se²⁻ was created in solution)

ii . Toluene was added to the above mixture at temperature of 45°C.

(The clusters grew up in nearby boundary face of toluene and solution.)

iii. The resultant greenish yellow solution of toluene

was concentrated and aged for a week.

The optical absorption spectra of (CdSe)_n were measured in toluene after illumination by xenon lamp combined with a monochromator to observe photo illumination effects.

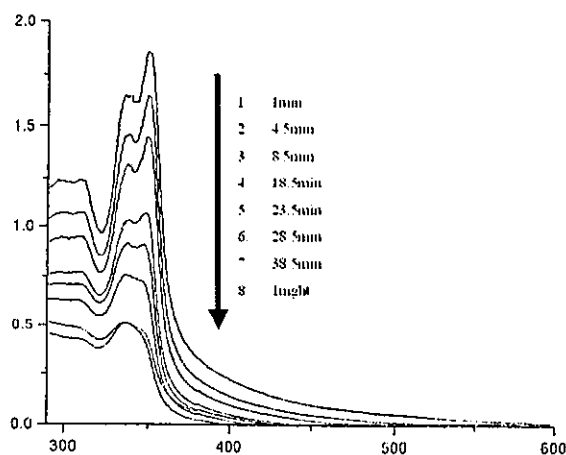


Fig. 1 Optical absorption spectra measured for the (CdSe)₁₃ sample in toluene. The abscissa is the light wavelength in units of nm and the ordinate is in arbitrary units. The eight curves (from up to bottom) correspond, respectively, to the observations after 1 min, 4.5 min, 8.5 min, 18.5 min, 23.5 min, 28.5 min, 38.5 min and 1 night light illumination of tungsten lamp after dissolving (CdSe)₁₃ in the solvent.

Figure 1 shows the optical absorption spectra of (CdSe)₁₃ clusters. The clusters also have the surfactant molecules, decylamine. It exhibits sharp peaks around 340-350nm. The eight curves in this figure represent the change of the observed spectra with the illumination times given in the figure. The uppermost curve is the

observation after 1 min of light illumination, while the lowermost curve is the observation of the clusters after its leaving for one night with the previous light illumination of the clusters by 38.5 min. As it is seen from the comparison of lowermost and its previous curves, the difference is negligible. It says that suspension of clusters is rather stable with a time, however its external perturbation by light source results in the changes of peak intensities and small blue-shift.

In order to investigate the $(\text{CdSe})_n$ clusters having time dependence, we have repeated calculations with the same cutoff energies for three different supercell sizes: $a = 16 \text{ \AA}$, 20 \AA and 24 \AA .

3. FIRST PRINCIPLE CALCULATION

We first performed structural optimization by means of the ultrasoft-pseudopotential program (VASP) [4] to obtain the locally stable wurtzite structure as well as the most stable endohedral cage structure that has already been done in Refs. [1-3]. The geometries of the resulting optimized $(\text{CdSe})_{13}$ clusters are shown in Figs. 2(a) and (b), respectively, for the endohedral cage and wurtzite structures, while the corresponding bulk geometries before relaxation are shown in Figs. 2(a') and (b'). The result for the endohedral cage structure is the same as that given in Refs. [1-3].

Note that there is no corresponding bulk geometry for the endohedral cage structure in Fig. 2(a).

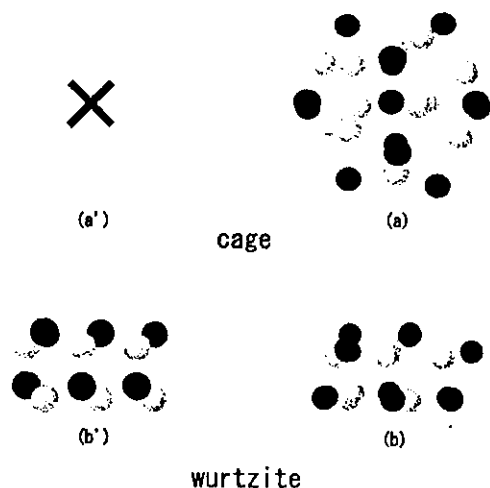


Fig. 2 Optimized $(\text{CdSe})_{13}$ geometries for the (a) endohedral cage and (b) wurtzite structures. Left figures, (a'), (b'), show the corresponding bulk geometries before relaxation (a cross in (a') means that the endohedral cage structure has no bulk counterpart). White and black spheres are Cd and Se atoms, respectively.

Next we performed the calculation of the dielectric function for the two clusters shown in Figs. 2(a) and (b). For this purpose, we used the all-electron mixed basis approach [5-7], in which each LDA wave function is expanded in the linear combination of both atomic orbitals (AO's) and plane waves (PW's). We used an

fcc lattice with the unit cell size corresponding to the nearest neighbor distance between clusters being equal to a . All core and valence AO's are generated by Herman-Skillman's atomic code [8] within the non-overlapping atomic spheres, and the 4 Ry is assumed for the PW's. The dielectric function is evaluated within the random phase approximation (RPA) via the equation [9]

$$\epsilon(q, \omega) = 1 - \frac{8\pi}{\Omega q^2} \sum_k \sum_{\lambda} \sum_{\nu} \frac{\langle k+q, \lambda | e^{iq \cdot r} | k, \nu \rangle^2 [f_0(\epsilon_{k+q, \lambda}) - f_0(\epsilon_{k, \nu})]}{\epsilon_{k+q, \lambda} - \epsilon_{k, \nu} - \omega - i\delta}, \quad (1)$$

where the summations with respect to the level indices λ and ν run over all levels (here we chose 1,000 levels), k is the wave vector inside the first Brillouin zone and denotes f_0 the Fermi-Dirac distribution function; the prefactor 2 means the spin multiplicity and Ω is the volume of the unit cell.

4. RESULT

Figs. 3(a) and (b) show our results of the dielectric function for the endohedral cage structure and wurtzite structure, respectively.

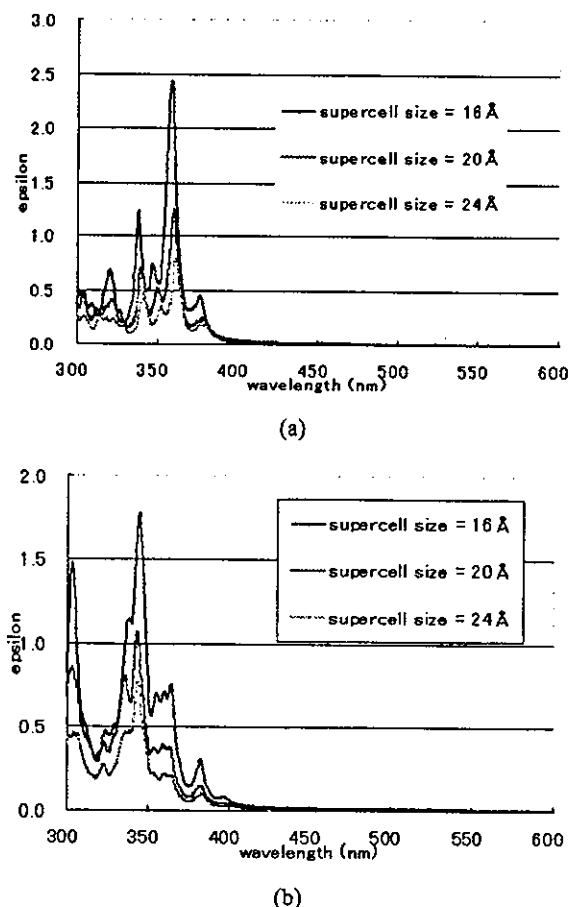


Fig. 3 Imaginary part of dielectric function of $(\text{CdSe})_{13}$ clusters for (a) the endohedral cage and (b) the wurtzite structures. In the figures, three curves (from top to bottom) represent the results for different supercell sizes, 16 \AA , 20 \AA and 24 \AA , respectively.

If we compare three curves in Figs. 3 (a) and (b), we find that the effect of the supercell size is not negligible, because the peaks of supercell size = 16 Å are much higher than those of supercell size = 24 Å. The larger the intercluster distance, the lower the height of the peaks. This is mainly because of the factor $1/\Omega$ in Eq.(1).

The peak positions are, however, not sensitive to the supercell size. In Fig. 3(a) for the endohedral cage structure, there are two peaks around 340nm and 360nm. On the other hand, the results for the wurtzite structure in Fig. 3(b) have the following characteristics:

- (1) Two peaks around 300-310nm and 340nm.
- (2) Shoulder around 350-360nm.
- (3) Long tail in lower energy side.

The shoulder of (2) may correspond to the right side of the experimental peaks around 350nm of lower curves in Fig. 1.

5. INTERPRETATION OF EXPERIMENT

Based on the fair agreements between theoretical calculation and experimental results, the observed spectra are interpreted as follows:

From the above result, under light illumination the certain number of clusters having cage like structure decomposes by a well-known effect of size selective photoetching. This seems to have a linear character with respect to the time of light illumination. The more the time of illumination, the more clusters decompose and a part of the rest of clusters changes the geometry from cage structure to wurtzite structure. It effects as well as to the local arrangement of the organic molecules surrounding $(\text{CdSe})_{13}$ which changes due to the electric fields caused by the charged rest of $(\text{CdSe})_{13}$ clusters. Then, we would imagine that the rest of clusters, solvent and surfactants molecules gradually rearrange their positions and structure to stabilize whole system.

The decrease of number of clusters leads to the increase of effective distance between $(\text{CdSe})_{13}$ clusters. Then, we could argue that the upper curves observed for low illumination times correspond to the samples that have a short intercluster distance and are characteristic of the endohedral cage structure, while the lower curves observed for long times illuminations correspond to the samples which have a large intercluster distance and are characteristic of wurtzite structure.

6. SUMMARY

In summary, we have optimized two (endohedral cage and wurtzite) structures of $(\text{CdSe})_{13}$ and calculated their

dielectric response function in the RPA on the basis of the LDA in density functional theory. We have compared its imaginary part with the optical absorption spectra measured experimentally for the $(\text{CdSe})_{13}$ sample dissolved in toluene. We conclude that most of the created clusters in solution have the endohedral cage structure. The experimental results show some aging effect of sample as noted in the optical spectrum. It may be caused by a change in the geometry of the clusters from the endohedral cage structure to the wurtzite structure. For this explanation, our theoretical results are consistent with the experimental observations. More experimental investigation, however, is necessary for sample preparation to discuss further. The calculations for the larger size cluster, of $(\text{CdSe})_{33}$ and $(\text{CdSe})_{34}$ is now on progress and will be reported in near future.

7. ACKNOWLEDGEMENT

The authors are grateful for continuous support of the HITAC SR8000 supercomputing facilities that are owned by the Computer Science Group at the Institute for Materials Research, Tohoku University. VK thankfully acknowledges the hospitality at the IMR and the support from JSPS.

REFERENCES

- [1] Y. Barnakov, R. Sivamohan, I. Dimitruk, T. Kudo, T. Nirasawa, T. Arai, K. Tohji, O. Terasaki, A. Kasuya, V. Kumar and Y. Kawazoe, Proc. Int. Symp. On Cluster Assembled Mater. (IPAP Conf. Series 3) pp. 56-58 (2002).
- [2] A. Kasuya, R. Sivamohan, Y. Barnakov, I. Dmitruk, T. Nirasawa, S. Mamykin, V. Romanyuk, K. Tohji, V. Jeyadevan, K. Shinoda, T. Kudo, O. Terasaki, Z. Liu, V. Kumar, R. Belosludov, V. Sundararajan, and Y. Kawazoe, to be published.
- [3] V. Kumar, R. Belosludov, V. Sundararajan, Y. Kawazoe, and A. Kasuya, to be published.
- [4] G. Kresse and J. Furthmüller, Comput. Mater. Sci. 6, 15 (1996); Phys. Rev. B 54, 11 169 (1996).
- [5] K. Ohno, Y. Maruyama, K. Esfarjani, Y. Kawazoe, N. Sato, R. Hatakeyama, T. Hirata and M. Niwano, Phys. Rev. Lett. 76, 3590 (1996).
- [6] K. Ohno, F. Mauri and S. G. Louie, Phys. Rev. B 56, 1009 ((1997).
- [7] S. Ishii, K. Ohno and Y. Kawazoe, Mater. Trans. JIM 40, 1209 (1999).
- [8] F. Herman and S. Skillman, "Atomic Structure Calculations" (Prentice-Hall, New Jersey, 1963).
- [9] S. L. Adler, Phys. Rev. 126, 413 (1962).

(Received October 13, 2003; Accepted April 24, 2004)

Dynamics on Electronic Excitation in Chemical Reaction

Takahiro Sawada¹, Jian Wu², Yoshiyuki Kawazoe³ and Kaoru Ohno¹¹Department of Physics Graduate School of Engineering, Yokohama, National University, 79-5 Tokiwadai, Hodogaya-ku, Yokohama 240-8501, Japan

Fax: 81-45-338-3020, e-mail: d03gd221@ynu.ac.jp, ohno@ynu.ac.jp

²Center for Advanced Study, Tsinghua University, Beijing 100084, P. R. China

Fax: 86-10-6278.1886, e-mail: wu@catu.tsinghua.edu.cn

³Institute for Materials Research, Tohoku University, Sendai 980-8577

Fax: 81-22-215-2052, e-mail: kawazoe@imr.edu

Carrying out simplified theoretical simulations using the time-dependent Schrödinger equation on the basis of the time-dependent density functional theory (for electrons) coupled with the Newtonian equation of motion (for nuclei), we find that a chemical reaction, $\text{Li}_2 + \text{H}_2 \rightarrow 2\text{LiH}$, takes place by the double excitation from the highest occupied molecular orbital (HOMO) level to the lowest unoccupied molecular orbital (LUMO) level. Along the reaction path, a level crossing occurs automatically between the highest occupied and lowest unoccupied levels and the electronic excited state changes smoothly into the electronic ground state leaving a kinetic energy of the molecules, i.e., a rapid energy transfer from the electronic excitation to the molecular motion of the order of 10 femto seconds.

Key words: time-dependent Schrödinger equation, spectral method, and a level crossing

1. INTRODUCTION

The electronic excitation opens new reaction channels of chemical reactions. It is interesting to study the chemical reactions at electronic excited states. When we simulate the dynamics on electronic excited states, we can avoid to use the potential energy surface (PES) [1,2] which is the most popular approach nowadays. Instead we can integrate directly the time-dependent *Schrödinger* equation (TDSE) within the framework of the time-dependent density functional (TDDF) theory [3,4]. The merit of doing it is to treat the wavepacket states as well as the steady states. In this paper we focus on the chemical reaction induced by double excitation in a simple system composed of Li_2 and H_2 and carry out the TDSE first-principle molecular dynamics (FPMD) simulation. In what follows, we present an explicit result of the dynamical simulation of $\text{Li}_2 + \text{H}_2 \rightarrow 2\text{LiH}$.

2. THEORY

In integrating the TDSE

$$i \frac{\partial}{\partial t} \Psi_j(t) = H(t) \Psi_j(t), \quad (1)$$

with respect to time, we introduce the spectral method [5]. This spectral method uses the eigenstate $\varphi_k(t)$ and the eigenvalue ε_j of the Hamiltonian $H(t)$, which satisfies

$$H(t) \varphi_k = \varepsilon_k \varphi_k. \quad (2)$$

Here, $H(t)$ denotes just the electronic part. Since it depends on time, this eigenvalue problem must be solved at each time. Therefore, φ_k and ε_k have also the time dependence, although it is not expressed explicitly. The oscillation of the Hamiltonian $H(t)$ may appear for time which is typically 100-1000 times smaller than the time step for the atomic motion and continue for a time interval of the order of a femtosecond. However, when

the electronic states are not far from steady states, the Hamiltonian would not significantly change in time inside this transient time interval. We expand the wavepackets $\Psi_j(t)$ in terms of the eigenstates $\varphi_k(t)$ at the same time,

$$\Psi_j(t) = \sum_k c_{jk}(t) \varphi_k, \quad (3)$$

where

$$c_{jk}(t) = \langle \varphi_k | \Psi_j(t) \rangle. \quad (4)$$

Hence, the basic time step Δt can be set as large as the time scale in which the Hamiltonian changes, one may integrate the TDSE as follows:

$$\Psi_j(t + \Delta t) = \sum_k c_{jk}(t) \exp(-i\varepsilon_k \Delta t) \varphi_k. \quad (5)$$

In real numerical treatments, the sum with respect to the eigenstates in Eq. (5) is evaluated only over a finite number of low-lying excited states as well as the ground state. Those low-lying excited states should include also the free-electron continuum states above the vacuum levels. So we use the all-electron mixed basis approach [6-8] which uses plane waves (PW's) together with atomic orbitals (AO's) as basis functions. The all-electron mixed basis approach enables us to represent correctly the free-electron continuum states as well as the bound and resonance states within the all-electron formalism. For the treatment of exchange-correlation terms, we use the local-density approximation (LDA). For the Newtonian equation of motion for nuclei, we use the forces calculated as a derivative of the total energy, as formulated by Ho et al. [9]

3. RESULT AND DISCUSSION

We first consider the case of the electronic ground state. Assuming zero initial velocity, we start the

TDSE-FPMD simulation. The initial atomic geometry of Li_2 and H_2 molecules are placed to face each other with a distance on the order of the bond length with which the molecules appears in the reaction. Figure 1 shows the time-evolution of atomic motion. The two molecules, Li_2 and H_2 , repel each other with slight intermolecular vibrations forming two isolated molecules. The trajectory is essentially the same as that obtained by the usual Car-Parrinello-type molecular dynamics simulation [4]. The time-evolution of the energy expectation values is shown in Fig. 2.

Next we consider the case of the doubly excited state from the highest occupied molecular orbital (HOMO) level to the lowest unoccupied molecular orbital (LUMO) level at the same initial geometry. The resulting trajectory [Fig. 3] is obviously quite different from the previous Fig. 1. This reaction yields two isolated LiH molecules. The motion of the atoms may be characterized as vibrations along the Li-H bond and repulsion between the LiH molecules. The initial H-H and Li-Li bond are broken very quickly. The balance of the Li-H bond is achieved near its ground-state bond length. The time-evolution of the energy expectation values is shown in Fig. 4 for doubly excited state.

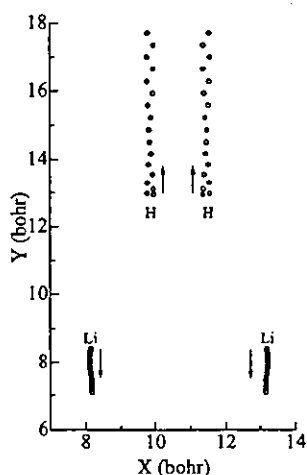


Fig. 1 The time evolution of atomic motion in the simulation starting from the ground state. The abscissa and ordinate represent, respectively, in the X and Y directions

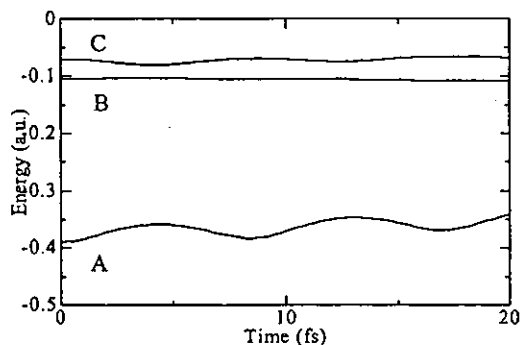


Fig. 2 The time-evolution of the energy expectation values of the valence electrons starting from the ground state. Level B is the highest occupied molecular orbital level. Level C is the lowest unoccupied molecular orbital level.

As seen in Fig. 4, a level crossing occurs between the highest occupied (C) and lowest unoccupied (B) levels approximately 10fs after the initial excitation. Since the present reaction proceeds nearly on the stationary state of the Hamiltonian at each time, it is possible to give a clear physical picture of the present reaction. We may consider only $1s$ orbital of H and $2s$ orbital of Li. Then, there are four possible electron levels, A, B, C and D, regardless of the spin multiplicity. First, level A has the lowest energy, representing the fully bonding molecular orbital (MO). Next, intermediate level B represents the bonding Li-Li and H-H and the anti-bonding Li-H MO, while level C represents the anti-bonding Li-Li and H-H and the bonding Li-H MO. Lastly, level D, having the highest energy, is characterized by the fully anti-bonding MO, although it is not shown in Figs. 2 and 4 because it exceeds the upper limit of vertical scale. Obviously there exists a bonding tendency between the Li and H atoms in levels A and C, and an anti-bonding tendency between the Li and H atoms in level B and D. Therefore, in the simulation starting from the ground state, in which level B is occupied and level C is empty, the two Li atoms attract each other and so do the two H atoms, because of the bonding tendency in the occupied levels A and B. On the other hand, in the simulation starting from the doubly excited state, in which level B is empty and level C is occupied, the Li and H atoms attract each other because of the bonding tendency in the occupied levels A and C. In fact, as shown in Fig. 4, levels A and C become closer to be degenerated and anti-bonding empty level B becomes higher when the Li and H atoms make bonds.

As a result of these bonding and anti-bonding tendencies, the level crossing occurs automatically when new molecules are synthesized. The occupied level C, which was originally higher than the empty level B, goes down due to the formation of the Li-H bonds and becomes lower than the empty level B without interlevel hopping. And the electronic energy plus potential energy between nuclei is lowered during this reaction, and the excess energy is all transferred into the kinetic energy of the atoms. In the way, the level crossing plays a key role in the process of the relaxation from the double excitation.

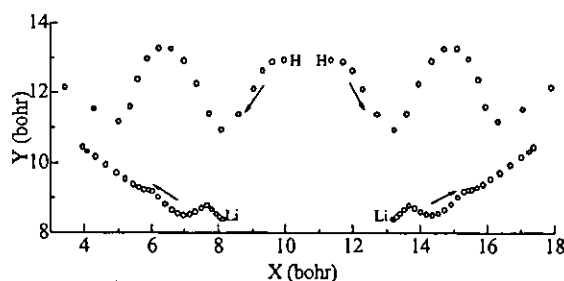


Fig. 3 The time evolution of atomic motion in the simulation starting from the doubly excited state

4. CONCLUSION

In this paper, by integrating the coupled equations of the TDSE-FPMD numerically with respect to time, we found a chemical reaction, $\text{Li}_2 + \text{H}_2 \rightarrow 2\text{LiH}$, in the double excitation. Along the reaction, a level crossing occurs between the HOMO and LUMO levels, according to Fukui's frontier orbital theory and Woodward-Hoffmann law [10-12]. From the present simulation, we can propose

a mechanism for relaxation of the reaction by the double excitation: electronic excited state changes smoothly into the electronic ground state leaving a kinetic energy of the atoms.

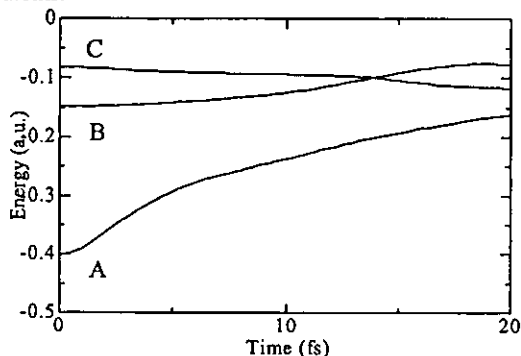


Fig. 4 The time-evolution of the energy expectation values of the valence electrons starting from the doubly excited state. By the double excitation, the electrons move from the highest occupied orbital level to the lowest unoccupied molecular orbital level. Level B is empty and levels A and C are occupied.

5. ACKNOWLEDGEMENT

The authors are grateful for the support of the HITAC SR8000 supercomputing facilities that are owned by the Computer Science Group at the Institute for Materials Research, Tohoku University.

REFERENCES

- [1] S. S. C. Ammal and P. Venuvanalingam, *J. Phys. Chem. A* **104**, 10859 (2000).
- [2] E. Bodo, Gianturco, R. Martinazzo and M. Raimondi, *Eur. Phys. J. D* **15**, 321 (2001).
- [3] E. Runge and E. K. U. Gross, *Phys. Rev. Lett.* **52**, 997 (1984).
- [4] see for a review, K. Ohno, K. Esfarjani and Y. Kawazoe, "Computational Materials Science", Solid-State Sciences, Vol. **129** (Springer-Verlag, Berlin, Heidelberg, 1999). : From Ab Initio to Monte Carlo Methods
- [5] J. J. Sakurai, "Modern Quantum Mechanics" (The Benjamin/Cummings Publishing Company 1985) Sect. 2.1
- [6] K. Ohno, F. Mauri, and S. G. Louie, *Phys. Rev. B* **87**, 1009 (1997).
- [7] T. Ohtsuki, K. Ohno, K. Shiga, Y. Kawazoe, Y. Maruyama and K. Masumoto, *Phys. Rev. Lett.* **81**, 967
- [8] S. Ishii, K. Ohno, Y. Kawazoe, and S. G. Louie, *Phys. Rev. B* **63**, 155104 (2001).
- [9] K. M. Ho, C. Elsässer, C. T. Chan and M. Fähnle, *J. Phys.: Condens. Matter* **4**, 5189 (1992).
- [10] K. Fukui, T. Yonezawa and H. Shingu, *J. Chem. Phys.* **20**, 722 (1952).
- [11] R. B. Woodward and R. Hoffmann, *J. Am. Chem. Soc.* **87**, 395 (1965).
- [12] J. Simons, "Quantum Mechanics in Chemistry" (Oxford Univ. Press, 1997)

(Received October 13, 2003; Accepted April 24, 2004)

Reprinted from

PHYSICAL REVIEW B

CONDENSED MATTER
AND MATERIALS PHYSICS

NOVEMBER 2004

15(I)

Water adsorption on Ti-doped silicon clusters

Hiroaki Kawamura,^{1,2} Vijay Kumar,^{1,3} and Yoshiyuki Kawazoe¹

¹*Institute for Materials Research (IMR), Tohoku University, 2-1-1 Katahira Aoba-ku, Sendai 980-8577, Japan*

²*New Frontiers Research Laboratories, Toray Industries, Inc., 1111 Teburo, Kamakura, Kanagawa 248-8555, Japan*

³*Dr. Vijay Kumar Foundation, 45 Bazaar Street, Chennai 600 078, India*

Published by
THE AMERICAN PHYSICAL SOCIETY

Volume 70

Third Series

Number 19

Water adsorption on Ti-doped silicon clusters

Hiroaki Kawamura,^{1,2} Vijay Kumar,^{1,3} and Yoshiyuki Kawazoe¹¹Institute for Materials Research (IMR), Tohoku University, 2-1-1 Katahira Aoba-ku, Sendai 980-8577, Japan²New Frontiers Research Laboratories, Toray Industries, Inc., 1111 Teburo, Kamakura, Kanagawa 248-8555, Japan³Dr. Vijay Kumar Foundation, 45 Bazaar Street, Chennai 600 078, India

(Received 10 February 2004; published 4 November 2004)

Ab initio calculations have been performed on adsorption of H₂O molecules on Ti-doped silicon clusters TiSi_n, using the ultrasoft pseudopotential method within the generalized gradient approximation. Our results show that for $n=13$ and larger clusters adsorption of H₂O on TiSi_n could be difficult due to low binding energies. All these clusters have cage structures with the metal atom surrounded by the silicon atoms. On the other hand, smaller clusters with $n < 13$ have the metal atom partially covered by Si atoms in a basket structure so that it is available for reaction with a water molecule. This leads to significantly higher binding energies of a water molecule on such clusters. These results are in excellent agreement with the available experimental data, which show significant decrease of H₂O adsorption on clusters with $n > 12$.

DOI: 10.1103/PhysRevB.70.193402

PACS number(s): 73.22.-f, 71.15.Nc, 61.46.+w

Currently, metal (M) encapsulated silicon clusters are attracting much attention¹⁻¹⁴ because of their interesting properties and structures. These could serve as building blocks for nanomaterials and miniature devices. Cage structures, especially fullerene, cubic, and Frank-Kasper type have been predicted for MSi_n ($n=14-16$) by Kumar and Kawazoe¹ with their unique characteristics. Subsequently, many theoretical studies have been made to determine the properties of clusters with $M=Cr$,²⁻⁴ Fe,^{1,5,6} and other M atoms.⁷⁻¹⁰ In addition, large abundances have been obtained for 15 and 16 Si atom clusters with one M atom^{11,14} and low reactivity of MSi_{12} , $M=Cr$, Mo, W has been obtained with hydrogen.^{3,12} Recently, adsorption behavior and electron affinities of Ti-doped clusters have been studied which are important for the understanding of their stability as well as for their usage. Kumar *et al.*¹³ have studied the ionization potentials and electron affinities of $M@Si_{16}$, $M=Ti$ and Zr clusters. Ohara *et al.*¹⁴ have reported the experimental results of not only the mass spectra but also the adsorption of H₂O molecules on Si_nTi clusters. These studies could also serve as important benchmarks to understand the structures of MSi_n clusters.

The results of these experiments show that adsorption of H₂O on Ti@Si_n clusters could be found only up to $n=12$. For larger clusters, the reaction ratio decreases significantly and from $n=15$ onwards it becomes almost zero. Considering the well known high reactivity of H₂O with Ti, the vanishingly small adsorption of H₂O molecules on TiSi_n clusters with $n > 12$ is thought to be due to the encapsulation of Ti by Si atoms so that Ti atom is not accessible to H₂O molecules for reaction. However, this idea could not explain all the experimental results *a priori*. For example, a hexagonal prism structure can exist for $n=12$ similar to the one^{3,12} for WSi₁₂. As the hexagonal faces are not capped, it is possible that H₂O could interact with Ti by intruding into the relatively open hexagonal rings. If it can, the experiments are not the proof for the formation of cage structures. Moreover, at the outset it is not clear if the Si atoms should be weakly interacting with H₂O if a cage is formed. The atomic structures of smaller clusters with $M=Ti$ have not yet been understood. In order to understand the interaction of H₂O with

TiSi_n clusters, the determination of the structures of TiSi_n clusters in the wide range of sizes under the same calculation conditions is indispensable. So far theoretical studies are mostly on a few selected sizes. Therefore, we have first performed calculations for determining the lowest energy structures of Ti@Si_n clusters with $n=8-16$. Based on these results, further calculations have been done on adsorption of a H₂O molecule on TiSi_n clusters.

The calculations are performed using the *ab initio* ultrasoft pseudopotential method,^{15,16} within the spin-polarized generalized gradient approximation of Perdew and Wang¹⁷ for the exchange-correlation energy. A simple cubic supercell with size 15 Å for $n=8-14$ and 18 Å for other larger clusters is used with periodic boundary conditions. The Brillouin zone is represented by the Γ point. For Si and O we consider only the outer valence electrons, but for Ti we also included 3*p* atomic core states as valence states. The structural optimizations have been performed using the conjugate gradient method such that the residual force on each ion was less than 0.001 eV/Å. The total energy has been calculated up to an accuracy of 0.0001 eV. In order to determine the lowest energy structures we used several candidates as initial guesses. Although one cannot still be completely sure of the minimum energy structures, we believe that our results should represent lowest energy structures. This belief is further supported by the good agreement with experiments of the adsorption behavior of a water molecule. Here we report the structures of TiSi_n, briefly from the point of view of the adsorption of H₂O. A detailed discussion of the low lying structures and the growth behavior has been given in Ref. 18. While under the experimental conditions of finite temperatures, there could be more than one isomer present for some clusters if the energy difference is small and vibrational contribution to entropy as well as zero point energy may affect the ordering of free energies, we have considered primarily the lowest energy structures. We believe that our studies demonstrate sufficiently clearly the main findings of the experiments.

Figure 1 shows the lowest energy structures of TiSi_n [(a)-(i)] and two interesting isomers [(j) and (k)] for TiSi₁₂ and TiSi₁₃, respectively. These can be classified into basket and

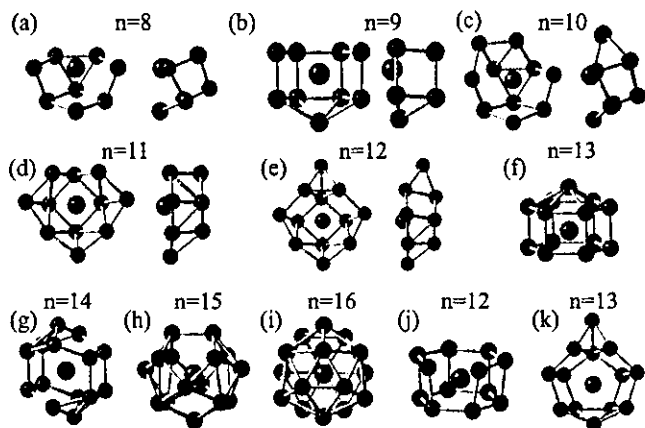


FIG. 1. (Color) (a)–(i) The lowest energy structures of TiSi_n ($n=8-16$) with (j) and (k) as the local minimum structures for TiSi_{12} and TiSi_{13} , respectively. Ti atom is shown by a bigger ball (green).

cage structures. As seen in Fig. 1, the most favorable structures for $n=8-12$ are basket type. In these clusters the Ti atom is partially covered with Si and therefore it could interact with H_2O . Furthermore, we find that a hexagonal prism structure is not the lowest energy structure for TiSi_{12} . It prefers a basket-type structure and it is the largest cluster for Ti@Si_n with the basket structure. Figure 1(j) shows a hexagonal prism-like cage structure for $n=12$, but one Si-Si bond is quite elongated (not bonded in Fig. 1), with the bond length of 3.00 Å. This can exist as a local minimum with 0.273 eV higher energy as compared to the basket isomer. The larger atomic radius of Ti as compared to Cr or W could be a reason for the opening of this hexagonal prism structure besides the fact that the number of electrons in the case of Ti is different, and this could also lead to a different structure to be of the lowest energy. We also calculated a hexagonal anti-prism structure and it lies 0.680 eV higher in energy. There-

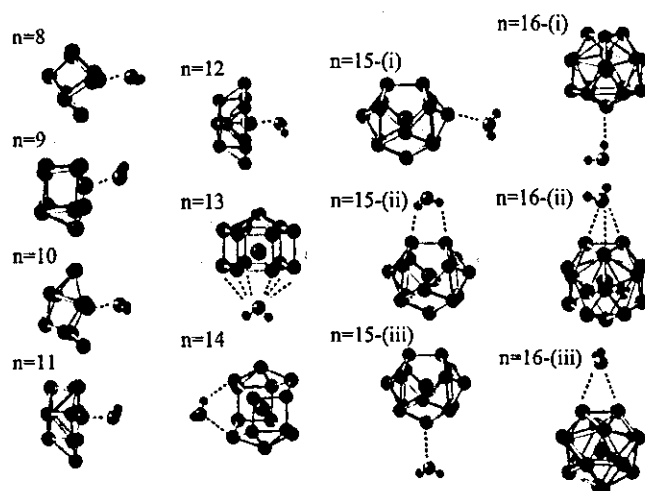


FIG. 2. (Color) Optimized arrangements of H_2O interacting with TiSi_n clusters. For $n=15$ and 16, three different approaches of water molecule to the cluster are shown. The nearest bonds between the H_2O and the cluster are shown by dashed lines. The small (big) balls represent H (O) atoms in the H_2O molecule.

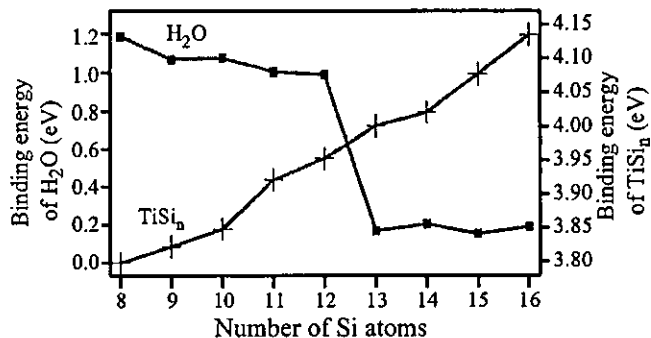


FIG. 3. Interaction energies (left scale) between TiSi_n and H_2O ($n=8-16$). The atomic arrangements for $n=15$ and 16 are shown, respectively, as 15-(i) and 16-(i) in Fig. 2 which have the largest interaction energy in each size. The right scale shows the binding energy per atom of TiSi_n clusters.

fore, it is also a local minimum isomer. From these results we conclude that cage structures are not suitable for $n=12$. Cage structures are, however, formed for $n > 12$ (Fig. 1). We calculated a basket isomer for $n=13$ [Fig. 1(k)] and it lies 0.878 eV higher in energy than the cage isomer. An interesting point is that $n=13$ and 14 have open (not capped) hexagonal rings so that H_2O molecule might intrude into the clusters to interact with Ti. Thus, the possibility of adsorption of H_2O molecules could not be determined only by these structures.

As in experiments of H_2O adsorption all clusters are positively charged, we also determined¹⁸ the structures of cation clusters following the results of the neutral clusters. It is found that the structural differences between the neutral and cation clusters are not significant. For $n=12$ the energy difference¹⁸ between the cage and the basket isomers is not large (0.273 eV) and we also studied cations of both these isomers. Our calculated energy difference between the cations is 0.387 eV and the basket isomer remains more stable than the cage isomer. More details of these studies will be published separately.¹⁸ The calculations of adsorption of H_2O on TiSi_n have been performed by initially putting an H_2O molecule with O facing the Ti atom of the lowest energy isomer of TiSi_n for $n=8-12$ (basket structures) and in front of the center of the open hexagonal ring for $n=13$ and 14 cage isomers. For $n=15$ and 16 cage isomers there are no such open sites for the H_2O molecule to adsorb. Therefore,

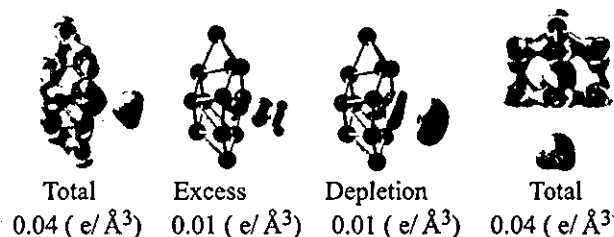


FIG. 4. (Color) Electronic-charge density isosurfaces for TiSi_n ($n=12$ and 13) interacting with H_2O . Excess and depletion charges for TiSi_{12} are calculated from the difference between the charge of TiSi_n interacting with H_2O and the sum of the charges of the isolated TiSi_n and H_2O .

TABLE I. Binding energy (BE) per atom for TiSi_n clusters, optimized distances between Ti and O ($d_{\text{Ti-O}}$), and interaction energies (E) between TiSi_n and H_2O . The three values for $n=15$ and 16 correspond to three configurations of H_2O . In the case of $n=13$, oxygen is nearly equidistant from Si and Ti atoms, but for $n=14-16$, the Ti-O bond is quite long and the interaction is actually with silicon atoms.

n	BE/atom (eV)	Optimized $d_{\text{Ti-O}}$ (Å)	E (eV)
8	3.798	2.14	1.188
9	3.822	2.16	1.069
10	3.848	2.16	1.076
11	3.921	2.20	1.004
12	3.953	2.19	0.989
13	4.001	3.78	0.169
14	4.021	4.52	0.204
15-(i)	4.077	5.64	0.152
15-(ii)	4.077	5.80	0.137
15-(iii)	4.077	6.03	0.078
16-(i)	4.135	6.26	0.189
16-(ii)	4.135	5.71	0.156
16-(iii)	4.135	5.87	0.156

three directions of approach have been selected for the H_2O molecule. The optimized arrangements and the distances between Ti and O are shown in Fig. 2 and in Table I, respectively.

In the basket isomers an H_2O molecule stays near the cluster and the distance between Ti and O after the optimization lies in the range of 2.14 to 2.20 Å. In the most important sizes of $n=13$ and 14, very weak or no adsorption could be found in experiments. It is found that in these cases the H_2O molecule moves away from the cluster and the final converged Ti-O bond lengths in $n=13$ and 14 are large (3.78 and 4.52 Å, respectively) and the interaction is more with the Si atoms. For $n=13$, the Si-O bond lengths are in the range of 3.65–3.71 Å, which are nearly equal to the Ti-O bond. However, the change in the position of Ti atom after adsorption of H_2O is quite small. Therefore, we conclude that interaction of H_2O is predominantly with Si atoms. In the case of $n=14$, the bare Ti@Si_{14} cage structure is quite distorted and O interacts with one Si atom such that the Si-O bond length is shorter (2.93 Å). In addition, one H interacts with a Si atom and the Si-H bond length is 2.61 Å. Accordingly in this case the interaction of H_2O is slightly stronger. This leads to a slight enhancement in the interaction energy. For Ti@Si_{15} and Ti@Si_{16} only weak interaction with Si atoms has been found for all three approaching directions, as expected. However, after optimization the directions of H_2O to the clusters are not the same. As seen in Fig. 2, for Ti@Si_{15} we considered two top sites and one bridge site as initial configurations with, O facing the cluster. In the two cases of top sites O interacts with the cage atoms [15-(i) and 15-(iii)], while in the case of the bridge site [15-(ii)], the two H atoms interact with the Si bridge atoms. The Si-H bond lengths are 2.92 and 3.15 Å. The O-Si bond lengths are 2.83 and 3.35 Å

for isomers 15-(i) and 15-(iii), respectively. For Ti@Si_{16} , O points to the cluster side when it is on a bridge site (Si-O bond lengths 3.50 Å) joining two Si hexagons [Fig. 2 (16-iii)] or on a triangle (Si-O bond lengths 3.48–3.58 Å) joining three Si hexagons [Fig. 2 (16-ii)]. However, when H_2O is placed on top of a capping atom (of Si hexagons), then H points towards the cluster, as shown in Fig. 2 (16-i) with Si-H bond length of 2.70 Å. The Si-H as well as Si-O bond lengths in these clusters are much longer as compared to the covalent bond length of about 1.5 Å for Si-H and 1.65 Å for Si-O. This different result indicates weak interaction between H_2O and the clusters.

In order to further quantify the interaction, we estimate the interaction energy from $E(\text{TiSi}_n) + E(\text{H}_2\text{O}) - E(\text{TiSi}_n + \text{H}_2\text{O})$. It is given in Table I and Fig. 3. The interaction energy in the basket isomers ($n=8-12$) is about 1 eV and except for $n=8$, it lies in a quite small range, the decrease being only 0.080 eV in going from $n=9$ to $n=12$. Therefore, adsorption of H_2O is energetically favorable for $n=8-12$, with a small decrease in the interaction energy as the size increases. On the other hand, the stability of clusters becomes better with an increase in size, as can be seen in Fig. 3. After $n=16$, there is a decrease in the binding energy.¹⁸ For $n=13-16$ the interaction energies of H_2O are less than about 0.20 eV and there is no significant difference with a change in n . It increases a little from $n=13$ to $n=14$, as also discussed above, and then decreases again. In experiments, a little adsorption has been found only in $n=13$ and 14 and there is also a little increase in going from 13 to 14.

From the above, it is therefore clear that our results are in excellent agreement with reported experiments and show that H_2O adsorption could occur up to $n=12$. The experimental results also show some interesting behavior of the reaction ratio, which agrees completely with our calculations. First, the experimental ratio decreases in going from $n=7$ to $n=12$, with the value changing from 0.8 to 0.4. Besides the small decrease in the interaction energy that we obtained in our calculations (Fig. 3), the structure is also likely to play an important role in adsorption. The most favorable structures of TiSi_n ($n=8-12$) are basket structures and with the increase in size, Ti atom loses its exposed part more and more, and finally at $n=12$, half of Ti is completely surrounded by Si atoms. Therefore, in such a structure, adsorption sites for H_2O become more limited so that the reaction ratio could decrease more significantly. The second interesting point is that in the experiment $n=13$ and 14 have still some reaction, while from $n=15$ the adsorption ratio is almost zero. As seen in Fig. 3, the inertness for adsorption is the same in $n=13-16$. However, considering the large structural change between $n=12$ and 13, the basket isomer for $n=13$ and 14 could exist even though cage isomer has an energetic advantage. The third interesting aspect is seen in $n=14$, which has larger adsorption ratio as compared to $n=13$. Our calculated results also show a slight increase in the interaction energy and this is likely to be responsible for an increase in the reaction ratio. In addition, $n=14$ cage isomer has two open hexagonal rings, while $n=13$ has one. A similar slight increase of the interaction ratio is seen for $n=10$ and there is a corresponding increase in the interaction energy as well.

$n=13-16$ clusters also have large highest occupied-lowest unoccupied molecular orbital gaps (more than 1.4 eV) and for $n=15$ and 16, it has values of 1.58 and 2.36 eV, respectively. This is also likely to be the reason for their inertness.

The bonding nature between TiSi_n and H_2O is important to understand adsorption behavior of H_2O molecules. To analyze the interaction we have plotted the electronic-charge density distributions in Fig. 4 for $n=12$ and 13 as representative examples of the adsorbing and not-adsorbing clusters, respectively. For $n=12$ we have shown the total, excess, and depletion of charge with the excess and depletion charges defined as the differences between the interacting system $\text{TiSi}_n+\text{H}_2\text{O}$ and the sum of charges of the isolated TiSi_n cluster and the H_2O molecule. From the total charge density distribution one finds strong covalent-like Si-Si bonds and some charge accumulation between Ti and H_2O . There is a small charge transfer from the vicinity of Ti and H ions to the region between the Ti and O ions. This charge transfer occurs in quite limited space so that the stability and the atomic structure of TiSi_n cluster is not affected significantly. For $n=13$ we have shown only the total charge density distribution as the excess and depletion charge distributions are too small (less than $0.01 e/\text{\AA}^3$). Therefore, the charge transfer as well as the interaction between TiSi_n cluster and H_2O molecule is rather weak, as expected.

The above description of interaction of water is corroborated by the orbital energies shown in Fig. 5. As one can see, the orbital energies of the TiSi_{12} cluster get shifted upwards, while those of H_2O molecule shift significantly to higher binding energies indicating significant covalent bonding between water and the silicon cluster. On the other hand for TiSi_{13} , this shift is quite small, supporting the weak interaction.

In summary, we have reported *ab initio* calculations of the adsorption of a H_2O molecule on titanium-doped silicon clusters of different sizes. The equilibrium structures and interaction energies have been obtained. It is found that TiSi_n clusters form a cage structure from $n=13$ onwards so that H_2O adsorption could occur only up to $n=12$, for which basket structures are preferred with Ti partially exposed and being available for interaction. These results are in excellent agreement with reported experimental results in which a little adsorption can be found beyond $n=12$. The interaction between TiSi_n and H_2O is evaluated by the calculation of the interaction energy. It clearly shows a decrease from $n=12$ to

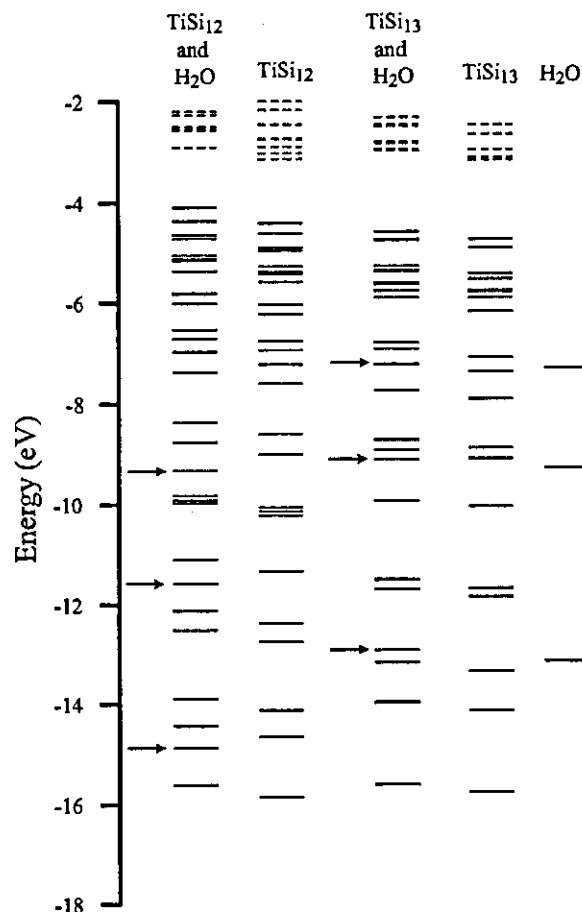


FIG. 5. Electronic levels for TiSi_n ($n=12$ and 13) before and after interaction with H_2O and the H_2O molecule. Broken lines show the unoccupied levels. The arrows show the position of the H_2O levels after adsorption.

$n=13$ and very small interaction energies for $n=14-16$, supporting their inertness and cage structures, in complete agreement with experiments.

V.K. thankfully acknowledges the kind hospitality at the Institute for Materials Research and the support from JSPS. We are grateful to the staff of the Center for Computational Materials Science at IMR for making Hitachi SR8000 super-computer available.

¹V. Kumar and Y. Kawazoe, Phys. Rev. Lett. **87**, 045503 (2001); **91**, 199901 (2003); V. Kumar, Eur. Phys. J. D **24**, 227 (2003); V. Kumar, Comput. Mater. Sci. **30**, 260 (2004).

²V. Kumar and Y. Kawazoe, Phys. Rev. B **65**, 073404 (2002); V. Kumar and Y. Kawazoe, Appl. Phys. Lett. **83**, 2677 (2003); V. Kumar *et al.*, Nano Lett. **4**, 677 (2004).

³V. Kumar and Y. Kawazoe, Phys. Rev. Lett. **90**, 055502 (2003).

⁴S. N. Khanna *et al.*, Phys. Rev. Lett. **89**, 016803 (2002).

⁵S. N. Khanna *et al.*, Chem. Phys. Lett. **373**, 433 (2003).

⁶G. Mpourmpakis *et al.*, Phys. Rev. B **68**, 125407 (2003).

⁷J. Lu and S. Nagase, Phys. Rev. Lett. **90**, 115506 (2003).

⁸F. Hagelberg *et al.*, Phys. Rev. B **67**, 035426 (2003).

⁹P. Sen and L. Mitos, Phys. Rev. B **68**, 155404 (2003).

¹⁰G. Mpourmpakis *et al.*, J. Chem. Phys. **119**, 7498 (2003).

¹¹S. M. Beck, J. Chem. Phys. **90**, 6306 (1989).

¹²H. Hiura *et al.*, Phys. Rev. Lett. **86**, 1733 (2001).

¹³V. Kumar *et al.*, Phys. Rev. B **68**, 155412 (2003).

¹⁴M. Ohara *et al.*, Chem. Phys. Lett. **371**, 490 (2003).

¹⁵G. Kresse and J. Furthmüller, Phys. Rev. B **54**, 11169 (1996); G. Kresse and J. Hafner, J. Phys.: Condens. Matter **6**, 8245 (1994).

¹⁶D. Vanderbilt, Phys. Rev. B **41**, 7892 (1990).

¹⁷J. P. Perdew and Y. Wang, Phys. Rev. B **45**, 13244 (1992).

¹⁸H. Kawamura, V. Kumar, and Y. Kawazoe, Phys. Rev. B (to be published).

Reprinted from

PHYSICAL REVIEW B

CONDENSED MATTER
AND MATERIALS PHYSICS

NOVEMBER 2004

15(I)

Nonicosahedral growth and magnetic behavior of rhodium clusters

Young-Cho Bae,¹ Hiroki Osanai,¹ Vijay Kumar,^{2,3} and Yoshiyuki Kawazoe²

¹*CODEC Co., Ltd., Kawasaki 215-0033, Japan*

²*Institute for Materials Research, Tohoku University, Aoba-ku, Sendai 980-8577, Japan*

³*Dr. Vijay Kumar Foundation, 45 Bazaar Street, K. K. Nagar (West), Chennai 600 078, India*

Published by
THE AMERICAN PHYSICAL SOCIETY

Volume 70

Third Series

Number 19

Nonicosahedral growth and magnetic behavior of rhodium clusters

Young-Cho Bae,¹ Hiroki Osanai,¹ Vijay Kumar,^{2,3} and Yoshiyuki Kawazoe²

¹CODEC Co., Ltd., Kawasaki 215-0033, Japan

²Institute for Materials Research, Tohoku University, Aoba-ku, Sendai 980-8577, Japan

³Dr. Vijay Kumar Foundation, 45 Bazaar Street, K. K. Nagar (West), Chennai 600 078, India

(Received 1 June 2004; revised manuscript received 23 July 2004; published 11 November 2004)

Ab initio pseudopotential calculations of the atomic structures and magnetic behavior of Rh_n ($n \leq 15$) clusters using the generalized gradient approximation for the exchange-correlation energy, reveal new lowest energy structures that are noncompact and have no atom at the center upto $n=13$, leading to a nonicosahedral growth. An eight-atom cluster has cubic structure and is magic. Some clusters beyond 13 atoms also do not have close packed structures due to some covalent character in the bonding. The calculated magnetic moments are generally lower and in better agreement with experiments than obtained before. Further studies on Ru_{13} and Pd_{13} clusters show that the lowest energy isomers of these clusters are also nonicosahedral. These findings of the novel behavior of technologically important transition metal clusters provide new ground for a better understanding and design of new catalysts.

DOI: 10.1103/PhysRevB.70.195413

PACS number(s): 36.40.Cg

I. INTRODUCTION

The occurrence of magnetism in clusters of nonmagnetic elements^{1,2} Ru, Rh, and Pd has attracted much attention in recent years³⁻⁸ but it is still not well understood. These elements lie in the periodic table just below the magnetic elements Fe, Co, and Ni, respectively, whose clusters have been found⁹ to have enhanced magnetic moments as compared to bulk due to reduced coordination of atoms and localization of electrons. Such an enhancement in magnetic moments also occurs on surfaces¹⁰ of magnetic elements where the coordination of atoms is again lower than in the bulk. The magnetic moments in these cases lie in between the values for the atom and the bulk. In clusters also, a large fraction of atoms lie on the surface and this leads to the development of magnetic moments in Ru, Rh, and Pd clusters. Earlier studies³⁻⁷ on clusters of these elements overestimated the magnetic moments as compared to the measured values¹ and obtained an icosahedral growth. However, here we report the finding of nonicosahedral growth in Rh clusters. These isomers generally have lower magnetic moments as compared to those reported before leading to a better agreement with experiments.

In addition to the fundamental interest in magnetism and bonding nature as well as their correlation with the atomic structures of nanoclusters, Rh clusters are important for catalysis¹¹ and it is necessary to know the atomic structures and magnetic properties properly to understand their role in reactions. Experiments¹ in the temperature range of 60–300 K suggest Rh_n clusters to be magnetic upto about $n=60$ with a value of $0.48 \pm 0.13 \mu_B/\text{atom}$ for Rh_{13} . *Ab initio* calculations have been done mostly on clusters having upto about 13 atoms. Studies using a tight binding model⁸ on clusters with n upto about 200 also showed icosahedral isomers to be lowest in energy. A spin-polarized density functional study^{3,4} of Ru, Rh, and Pd clusters having upto 147 atoms showed large magnetic moments on small clusters and icosahedral growth to be lowest in energy. For Ru and Rh the magnetic moments were found to decrease much

faster as compared to Pd with an increase in the cluster size. The magnetic moment on Rh_{13} in an icosahedral structure has been calculated to be 1.62 and $1.15 \mu_B/\text{atom}$, respectively, by Reddy *et al.*⁵ and Reddy *et al.*⁶ Jinlong *et al.*⁷ also obtained $15 \mu_B$ magnetic moment on Rh_{13} using the discrete variational method while Kumar and Kawazoe⁴ obtained $21 \mu_B$ magnetic moment on this cluster. However, it was shown⁴ that isomers with lower magnetic moments such as the one with $15 \mu_B$ lie only about 0.04 eV higher in energy and therefore lower magnetic moment isomers are expected to be present in experimental conditions. These results generally show that the calculated values are significantly higher than those obtained from experiments. Reddy *et al.*⁶ obtained structures using a parametrized model potential without spin polarization. The resulting structures were reoptimized using density functional calculations. Guirado-Lopez *et al.*⁸ kept the symmetry of the clusters fixed. Our *ab initio* calculations surprisingly reveal noncompact and nonicosahedral structures to be energetically more favorable opening a new possibility in the understanding of this important class of clusters. A non-icosahedral growth has also been obtained¹² for Nb clusters. Therefore, we performed further checks on the structures of Ru_{13} and Pd_{13} clusters. Interestingly we find an icosahedron for Ru_{13} to be much higher in energy as compared to the non-compact structure while for Pd_{13} the noncompact structure is lower in energy but it is nearly degenerate with an icosahedron.

II. METHOD

The calculations have been performed using the *ab initio* ultrasoft pseudopotential plane wave method.^{13,14} The cutoff energy for the plane wave expansion is taken to be 205.5, 203.6, and 199 eV for Rh, Ru and Pd, respectively. The generalized gradient approximation (GGA)¹⁵ with spin polarization has been used for the exchange-correlation energy and the Γ point, for the Brillouin zone integrations. Several structures have been fully optimized using the conjugate gradient

method such that the force on each ion became less than 0.005 eV/\AA . The energy is converged to an accuracy of 0.0001 eV . In most cases the low lying isomers are further checked for different spin-isomers using a constraint on the net magnetic moment and the reoptimization of the atomic structure. The binding energy (BE) of Rh_2 is calculated to be 2.04 eV/atom with the bond length of 2.20 \AA . The magnetic moment reduces to $2\mu_B/\text{atom}$ from the atomic value of $3\mu_B$. There is a large scatter in the available theoretical values for a dimer. We compare our results with those obtained by using GGA. Our BE (bond length) is slightly higher (shorter) as compared to 1.88 eV/atom (2.34 \AA) obtained⁶ by using DMOL and GGA. Also our BE is higher than the experimental value¹⁶ of 1.46 eV/atom but the bond length is in better agreement with the experimental value of 2.28 \AA . The bulk cohesive energy and lattice constant for Rh are calculated to be 6.06 eV/atom and 3.83 \AA that are in good agreement with the experimental values of 5.75 eV/atom and 3.80 \AA , respectively. Therefore, we expect a better prediction of the BEs of clusters with increasing size but an overall slight overestimation.

III. RESULTS

A. Structures

The low lying isomers of Rh_n clusters with $n=4-12$ are shown in Fig. 1. The BEs, magnetic moments, and mean nearest neighbor bond lengths of the lowest energy isomers are given in Table I. Earlier studies^{6,7} have reported a tetrahedral structure for Rh_4 with $4\mu_B$ magnetic moment. This is nearly degenerate with a nonmagnetic tetrahedral isomer. We find a bent (nearly 90°) rhombus (side 2.41 \AA , angles 71.9° and 70.4° , and diagonals 2.78 and 2.83 \AA) to be lowest in energy with $6\mu_B$ magnetic moment while a square (side 2.33 \AA) lies 0.15 eV higher in energy with $4\mu_B$ magnetic moment. A tetrahedron (side 2.45 \AA) lies 0.19 eV higher in energy and is nonmagnetic. This is the first result for transition metal clusters that an open structure has lowest energy. For Rh_5 , we obtain a square pyramidal structure (bond lengths 2.42 \AA in the base and 2.54 \AA from vertex to base) with $5\mu_B$ magnetic moment to be 0.31 eV lower in energy than a trigonal bipyramid (bond lengths 2.65 \AA in the base and 2.50 \AA from vertex to base) that has $7\mu_B$ magnetic moment. A similar result was obtained earlier.⁶ For Rh_6 a slightly distorted prism with mirror symmetry (bond length varying between 2.36 to 2.47 \AA with the mean value of 2.43 \AA) and an octahedron (bond length varying from 2.50 to 2.66 \AA with the mean value of 2.54 \AA) each with $6\mu_B$ magnetic moment are nearly degenerate while a bi-capped tetrahedral structure lies 0.31 eV higher in energy with $10\mu_B$ magnetic moment. A nonmagnetic octahedral isomer lies only 0.05 eV higher in energy than the $6\mu_B$ isomer and therefore in this octahedral isomer the magnetic behavior is very weak and can be easily destroyed even at quite low temperatures. However, the nonmagnetic prism isomer lies 0.22 eV higher in energy and therefore it is unlikely to be observed at room temperature. An isomer with the capping of the lowest energy Rh_5 pyramid structure lies 0.55 eV higher in energy with $4\mu_B$ magnetic moment. We also calcu-

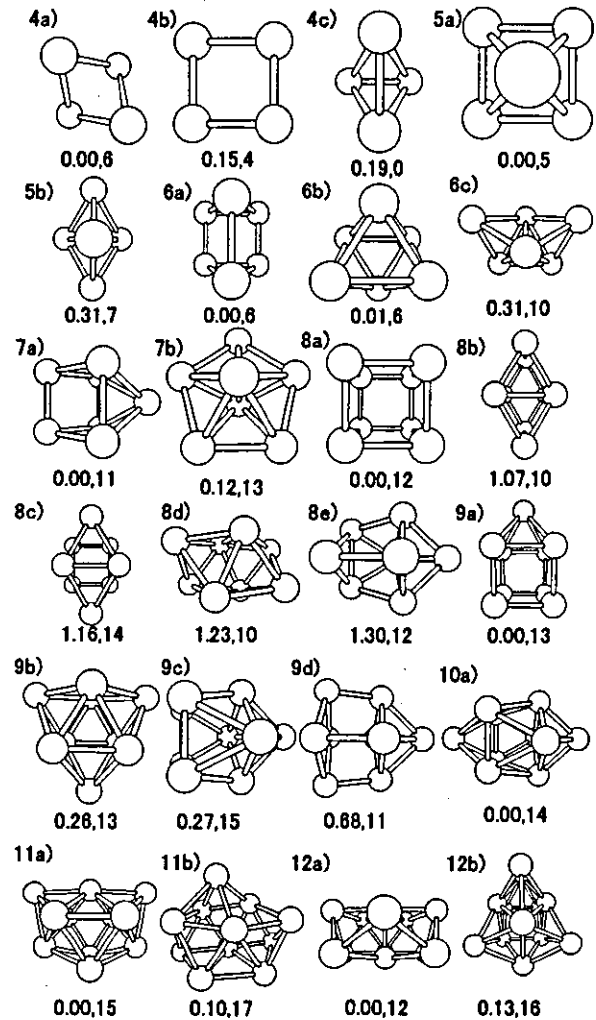


FIG. 1. Atomic structures of Rh_n clusters with $n=4-12$. Isomer (a) has the lowest energy which is taken as reference. The relative energies (eV) of other isomers are given below each structure along with the magnetic moment in the unit of μ_B . The structure of 12a has six atoms in each layer. There is one atom in the center of the upper layer to which two side atoms are connected. The front atom in this layer is connected with two atoms in the lower layer. The latter also has one atom behind the central atom. The smaller the size of the ball, the deeper is the position.

lated a planar triangular structure and a hexagon. These lie 2.08 and 3.38 eV higher in energy with 8 and $0\mu_B$ magnetic moments, respectively than the lowest energy isomer. Therefore, these low dimensional structures lie significantly higher in energy for $n=6$. Earlier an octahedral structure was obtained for this cluster. However, our finding of the prism structure is important as for Rh_7 also we find a square capped prism structure with $11\mu_B$ magnetic moment to be 0.12 eV lower in energy than a pentagonal bipyramid ($13\mu_B$) obtained before.^{6,7} An isomer in which a triangular face of the prism is capped lies 0.48 eV higher in energy with $7\mu_B$ magnetic moment.

Another surprising finding is that Rh_8 has a perfect cubic structure with 2.40 \AA side and $12\mu_B$ magnetic moment. The bond length is quite short and it reflects the strong covalent bonding in this cluster. It lies about 1 eV lower in energy

TABLE I. The binding energy (BE), magnetic moment (M), and mean nearest neighbor bond lengths (d) in the lowest energy isomers of Rh clusters.

n	Structure	BE (eV/atom)	M (μ_B)	d (Å)
4	Bent rhombus	3.12	6	2.41
5	Square pyramid	3.40	5	2.48
6	Prism	3.57	6	2.43
7	Capped prism	3.71	11	2.50
8	Cube	3.96	12	2.40
9	Capped cube	3.97	13	2.47
10	Bicapped tetragonal antiprism	4.02	14	2.56
11	Fused pentagonal pyramids	4.06	15	2.57
12	Bilayers	4.12	12	2.55
13	Cage	4.16	17	2.57
14	capped hexagonal prism-like	4.23	16	2.55
15	Hexagonal	4.26	19	2.62

than many other isomers [8(b)–8(e) in Fig. 1] such as two prisms fused on a square face, a bicapped prism, a D_{2d} type structure, and a capped pentagonal bipyramid that are 1.07, 1.16, 1.23, and 1.30 eV higher in energy with 10, 14, 10, and $12\mu_B$ magnetic moments, respectively. As we shall show later, this cluster shows magic behavior. Among transition metal clusters, eight-atom cluster of Nb has also been found¹² to be magic but the lowest energy structure of Nb₈ is a bicapped octahedron. These results indicate that the close packed structures of Rh clusters are not of the lowest energy and the growth behavior in this size range does not follow the partial icosahedral structure route. In fact the capped pentagonal bipyramid structure lies highest in energy among these isomers. Furthermore a tetrahedron with four faces capped and a hexagonal bipyramid of Rh₈ lie 2.09 and 2.92 eV higher in energy with 12 and $0\mu_B$ magnetic moments, respectively.

The above growth behavior is continued further and Rh₉ is a capping of cubic Rh₈ with $13\mu_B$ magnetic moments. It is quite different from a bicapped pentagonal bipyramid obtained earlier.⁶ We obtain a capped tetragonal antiprism (9c) to be 0.27 eV higher in energy. It has $15\mu_B$ magnetic moment. This can also be considered as a pentagonal prism capped with a triangle on one side. A capped tetragonal prism type isomer (9d) lies 0.68 eV higher in energy and is unlikely to be present in experiments. We also obtained a tricapped prism (9b) which is 0.26 eV higher in energy and has $13\mu_B$ magnetic moments. Therefore, our results are the lowest spin isomers. However, for Rh₁₀, our result of bicapped tetragonal antiprism (10a) ($14\mu_B$ magnetic moments) is the same as obtained before.⁷ A bicapped distorted hexagonal biprism lies 0.30 eV higher in energy with $16\mu_B$ magnetic moments whereas a bicapped (opposite faces) cube and two interconnected pentagonal bipyramids lie significantly higher (0.95 and 1.19 eV) in energy with 10 and $12\mu_B$ magnetic moments, respectively. Several different cappings of a

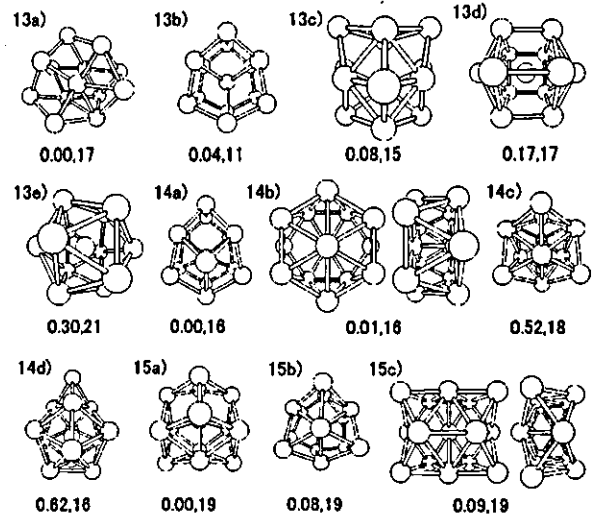


FIG. 2. The same as in Fig. 1 but for $n=13-15$.

pentagonal bipyramid were also optimized and these lie 0.5 eV or higher in energy, supporting the non-icosahedral growth in these clusters.

The lowest energy isomer of Rh₁₁ (11a) can be viewed as two capped pentagons joined by an atom. It has $15\mu_B$ magnetic moments. Another low lying isomer (11b) can be viewed as capped two layers of five atoms each (five atoms in a triangular packing in one layer and a pentagon in another). It lies only 0.10 eV higher in energy and has $17\mu_B$ magnetic moments. It is likely to be present in experiments. This structure is a precursor to the lowest energy structures of Rh₁₂ and Rh₁₃. There is no atom at the center. Similarly for $n=12$, a two layer structure (12a) has the lowest energy. It has mirror symmetry and $12\mu_B$ magnetic moments. Increasing or decreasing the magnetic moments of this cluster by $2\mu_B$ makes only a small change in energy of about 0.1 eV and therefore, the magnetic moments can be easily affected by temperature. There are slightly different isomers. One is shown in Fig. 1 (12b) and it lies only 0.13 eV higher in energy and should also be present in experiments. It also has a mirror symmetry with the magnetic moments of $16\mu_B$. So in this case, it can be possible that there is an increase in the magnetic moments with an increase in temperature.

The most important result is obtained for Rh₁₃. Earlier an icosahedron has been reported to be lowest in energy.⁴⁻⁷ We carried out optimizations for icosahedron, cuboctahedron, decahedron, and capped cubic structures as well as several other isomers. A few low lying isomers are shown in Fig. 2. Surprisingly a cage structure (13a) with $17\mu_B$ magnetic moment and no atom at the center is 0.30 eV lower in energy than an icosahedron (13e) with $21\mu_B$ magnetic moment as obtained before.⁴ (An icosahedral isomer with $17\mu_B$ magnetic moment is only about 0.01 eV higher in energy and is almost degenerate.) It has a pentagon (in the middle), a rhombus on one side, and a near square on the other. These results indicate that in general, Rh clusters prefer relatively open structures. Several other atomic and spin isomers lie close in energy. This will also lead, in general, to spin isomers with lower magnetic moments to be present in experiments. There is an isomer (with mirror symmetry) (13b)